Analysis of Singularity Properties of the Radiation Field in Low-Mode Optical Fibres

Alexeyev A.N., Alexeyev C.N., Fadeyeva T.A. and Volyar A.V.

Physics Department, V.I. Vernandsky Taurida National University
4 Vernadsky Ave., 95007 Simferopol, Crimea, Ukraine
e-mail: volyar@ccss.crimea.ua

Received 17.11.2005

Abstract

We analyze the physical processes in optical fibres on the basis of the radiation field emitted from the output end. It is demonstrated that one can judge about the excitation coefficients of the guided modes in ideal optical fibres from the position of singularity point and equal intensity lines. We have obtained dependence of the excitation coefficients of guided optical vortices (OV) upon the displacement of the OV incident on the input fibre end. It is shown that the motion of the singularity point at the output end is caused by the rotational Doppler effect.

Key words: optical vortex, singularity, optical fibre

PACS: 41.85.-p; 42.81.-i; 47.32.Cc

1. Introduction

It is well-known [1–3] that the radiation field of low-mode optical fibres exhibits usually a presence of singularity points, whose position depends on excitation conditions [4], external perturbations [2] and orientation of polarizer placed after the output end of the fibre [5]. The only way to analyze the processes in a fibre is studying radiation field of that fibre. It is often necessary to know the mode state and the weight of each mode excited in the fibre. Hitherto the mode composition has been often analyzed qualitatively, by means of comparing the radiation pattern with numerically simulated intensity distributions [6]. The method of partial waves has also been applied in order to calculate the amplitude excitation coefficients of the modes with the same azimuthal (l) and radial (m) indices, based on the radiation pattern observed in the far field zone of a lens [7]. However, intensity distributions at the output end of fibre are also affected by the mode dispersion arising within the mode group. That is why the method described in [7] does not allow one to calculate the weights of different fibre modes with a necessary accuracy. It is used while analyzing the radiation field in multimode fibres, where the inter-mode dispersion prevails. In low-mode fibres, where only few (two in our case) mode groups with the same indices can be excited, the method is inapplicable. The technique used in the work [8] enables one to calculate the mode weights both for different mode groups and within a group with the same orbital index l in low-mode fibres, where a singularity is present in the radiation field.

On the other hand, great efforts have recently been made for studying the rotational Doppler effect (RDE) [9], which renders different frequency shifts for optical vortices (OV) and Gaussian beams [10,11]. The cases studied earlier have been concerned only with the beams having the same homogeneous polarization.

This is why the frequency of the singularity rotation has been determined from the topological charge of the OV. In case of the radiation field of optical fibres, its constituents have different polarizations and, therefore, the manifestations of the RDE would also depend upon the polarizations and weights of the constituent modes.

The aim of the present work is to determine dependence of the weight coefficients of modes in an ideal optical fibre on the conditions of its excitation. We also study manifestations of the RDE in low-mode fibre characterized with the waveguide parameter V<3.8 under the excitations of different types.

2. Excitation coefficients of guided fibre modes

Let a circularly polarized Laguerre-Gaussian beam that bears a unit OV be incident at the entrance face of a round isotropic fibre. Let its centre be shifted from the fibre axis and be located at the point (x_0,y_0). We assume that the angle between the fibre and the beam axes is equal to u and the projection of the beam axis makes an angle θ with respect to the x axis. In the conditions of small u values (e.g., several degrees, corresponding to quite real cases of the fibre excitation), the field of the incident beam may be represented in the form

$$\mathbf{E}_{\mathbf{t}} = \hat{\mathbf{e}}^{\pm}\left[(x-x_0)\pm i(y-y_0)\right]\exp\left\{-\frac{(x-x_0)^2+(y-y_0)^2}{2\rho_g}+iku\left(x\cos\theta+y\sin\theta\right)\right\}, \quad (1)$$

where ρ_g is the waist radius.

The fibre eigenmodes at the input end (z=0) written in the basis of circular polarizations read as

$$\mathbf{e}_{\mathbf{t}\pm l} = \hat{\mathbf{e}}^{\pm}F_l(R)\exp\{\pm il\varphi\}, \quad (2)$$

where $R = r/\rho$, r,φ denote the cylindrical polar coordinates, ρ the core radius, and the signs referred to the superscripts of the unit vectors and the topological charge of OV (l=0,1) are independent. Consider a case of parabolic distribution of the refractive index ($n^2 = n_{co}^2\left(1-2\Delta\left[r/\rho\right]^2\right)$, $(r<\rho)$), whereas the radial dependence of modes (see [12]) is defined by

$$F_l(R) = R^l\exp\left\{-\frac{1}{2}VR^2\right\}. \quad (3)$$

Since the guided vortices described by Eq. (2) form an orthogonal basis, one can decompose the transverse field in terms of the fibre eigenmodes:

$$\mathbf{E}_{\mathbf{t}} = \sum_j a_j\mathbf{e}_{\mathbf{t}j}\ . \quad (4)$$

Upon multiplying Eq. (4) by $\mathbf{e}_{\mathbf{t}l}^*$ and subsequently integrating over the cross section S_∞, one can obtain the mode excitation coefficients [12]:

$$a_l = \int_{S_\infty}\mathbf{E}_{\mathbf{t}}\cdot\mathbf{e}_{\mathbf{t}l}^*(\rho,\phi)\,dS \Big/ \int_{S_\infty}\left|\mathbf{e}_{\mathbf{t}l}\right|^2 dS\,. \quad (5)$$

Let us denote hereafter the denominator of Eq. (5) as N_l.

Due to orthogonality of the unit vectors $\hat{\mathbf{e}}^{\pm}$, circularly polarized incident beam can excite in the fibre only three modes with the same polarization. From Eqs. (1)–(5) one gets the following excitation coefficients:

$$a_{+1} = \frac{2V^2}{\rho^3\rho_g\left(1+\dfrac{V\rho_g^2}{\rho^2}\right)^2}\left[\frac{\left(x_0+iku\rho_g^2\cos\theta\right)^2+\left(y_0+iku\rho_g^2\sin\theta\right)^2}{\left(\dfrac{1}{\rho_g^2}+\dfrac{V}{\rho^2}\right)}+\rho_g^4\left(2-iku\left(x_0+iy_0\right)e^{-i\theta}\right)-\rho_g^2\left(x_0^2+y_0^2\right)\right]$$

$$\times\exp\left\{\frac{\left(x_0+iku\rho_g^2\cos\theta\right)^2+\left(y_0+iku\rho_g^2\sin\theta\right)^2}{2\rho_g^2\left(1+V\rho_g^2/\rho^2\right)}-\frac{x_0^2+y_0^2}{2\rho_g^2}\right\},$$

$$a_{-1}=\frac{2V^2}{\rho^3\rho_g\left(1+\frac{V\rho_g^2}{\rho^2}\right)^2}\left[\frac{\left\{\left(x_0+iku\rho_g^2\cos\theta\right)+i\left(y_0+iku\rho_g^2\sin\theta\right)\right\}^2}{\left(\frac{1}{\rho_g^2}+\frac{V}{\rho^2}\right)}-\rho_g^2\left(x_0+iy_0\right)\left\{\left(x_0+iy_0\right)+iku\rho_g^2e^{i\theta}\right\}\right] \tag{6}$$

$$\times\exp\left\{\frac{\left(x_0+iku\rho_g^2\cos\theta\right)^2+\left(y_0+iku\rho_g^2\sin\theta\right)^2}{2\rho_g^2\left(1+V\rho_g^2/\rho^2\right)}-\frac{x_0^2+y_0^2}{2\rho_g^2}\right\},$$

and

$$a_0=\frac{2V\rho_g}{\rho^2\left(1+\frac{V\rho_g^2}{\rho^2}\right)^2}\left[\left(x_0+iy_0\right)\left\{1-2\left(1+\frac{V\rho_g^2}{\rho^2}\right)\right\}+iku\rho_g^2e^{i\theta}\right]$$

$$\times\exp\left\{\frac{\left(x_0+iku\rho_g^2\cos\theta\right)^2+\left(y_0+iku\rho_g^2\sin\theta\right)^2}{2\rho_g^2\left(1+V\rho_g^2/\rho^2\right)}-\frac{x_0^2+y_0^2}{2\rho_g^2}\right\}.$$

The power per mode may be found in the form (see [12])

$$P_i^{x,y}=\frac{n_{co}}{2}\sqrt{\frac{\varepsilon_0}{\mu_0}}\frac{\left|\int\limits_{S_\infty}E_{ti}\cdot\left(e_{tl}\right)^*dS\right|^2}{\int\limits_{S_\infty}\left|e_{tl}^i\right|^2dS}. \tag{7}$$

The curves for the mode power as a function of x_0 and u are displayed in Fig. 1. It is obvious from Fig. 1 that the power of the excited OV decreases with increasing either x_0 or u, whereas the power of the other vortex and the fundamental mode first increases and then decreases. Besides, the power of the initial vortex is larger than the resulting power of the other two modes, which agrees well with the results [13].

Experimental investigations have been carried out by means of setup shown schematically in Fig. 2. A light from He-Ne laser (the wavelength of λ=0.63 μm) passes through polarizer P_1 and a quarter-wave plate $\lambda/4$, which changes the sign of polarization of the light. Then the beam propagates in an optical wedge (OW) formed by a covering glass OW, which generates the OV at the output [14]. After the OW, the light passes through a semitransparent mirror, a 20^x microobjective MO_1 and is then directed into a 1 m quartz fibre F with the waveguide parameter of V=3.6. A part of the

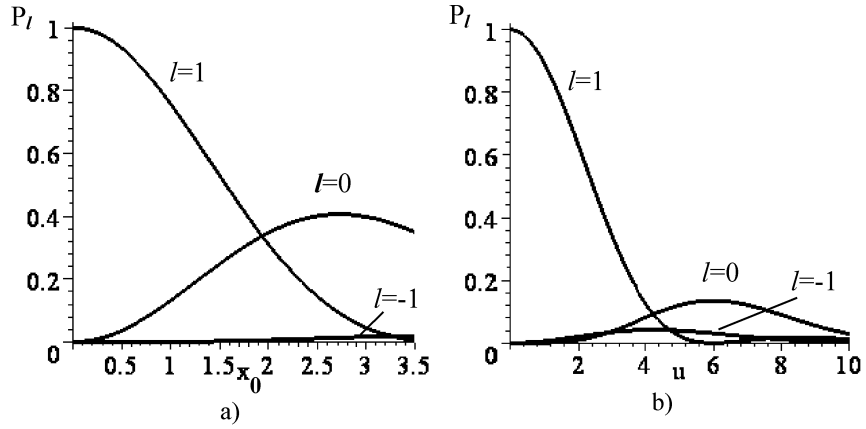

Fig.1 Power of the partial mode versus displacement x_0 (a) and inclination angle u (b).

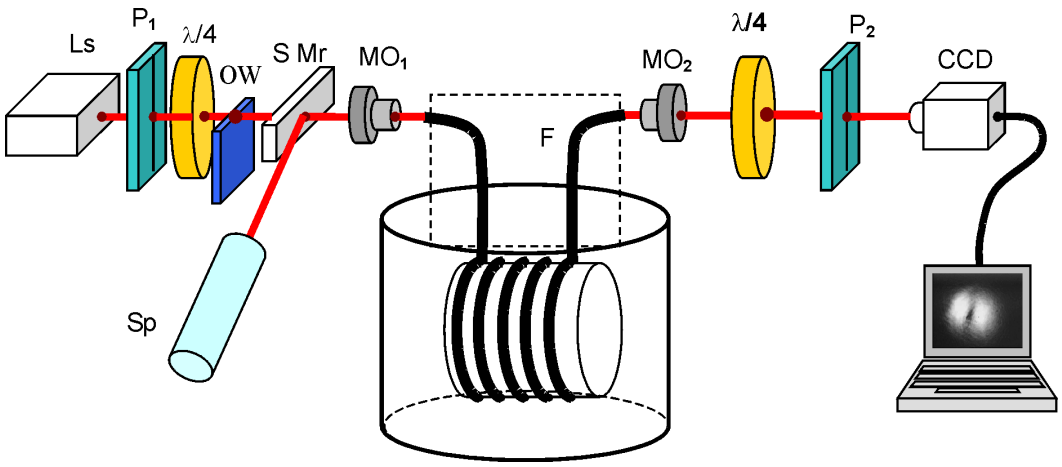

Fig. 2 Schematic representation of experimental setup. Ls – He-Ne laser, S Mr – semitransparent mirror, □/4 – quarter-wave retarder, $P_{1,2}$ – polarizers, $MO_{1,2}$ – 20, 8^x microobjectives, OW – optical wedge, F – optical fibre, Sp – spyglass, CCD – CCD camera, and PC – personal computer.

beam reflected from the input face of the lens of MO_1 interferes with the beam reflected from the input face of the fibre and is put into the spyglass by means of semitransparent mirror. The alignment of the laser beam and the fibre axis could be checked using the beam reflected from the input face of the microobjective MO_1. The tuning error has been equal to 2^o. The laser spot has been displaced with respect to the fibre face by means of 0.5 μm-pitch microshift device, whose input end is fixed. The excitation has been monitored with a side-view microscope consisting of a semitransparent mirror and a spyglass. At the output end of the fibre, the setup includes, one after another, another 8^x microobjective (MO_2), a λ/4 plate and an analyzer (P_2), which transmits the initial polarization and cuts off the orthogonal component caused by energy transfer to the *IV* vortex. Then the image is projected onto CCD camera connected with computer. We have processed the obtained images with a special program according to the technique described in the study [8]. The experimental values of normalization coefficients $a_i^n = a_i \Big/ \left[a_0^2 + a_1^2 + a_{-1}^2 \right]^{1/2}$ are given in Fig. 3, where the results predicted theoretically by Eq. (6) are plotted as solid lines. As seen from Fig. 3, there is good agreement between our theoretical and experimental data.

3. Rotational Doppler effect in optical fibres

Let us now consider the system consisting of the optical fibre (the waveguide parameter V<3.8), which sustains only the modes with the azi-

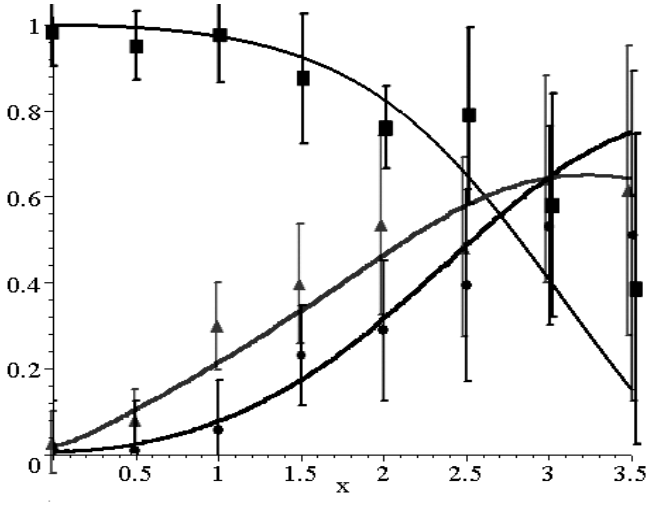

Fig. 3. Normalized excitation coefficients of the guided OV versus displacement *x*. Experimental results: ● – a_0^n, □– a_1^n, △– $a_{-1}^{\prime n}$. Theoretical curves are plotted in solid lines.

muthal indices l=0 and 1 (HE_{11}^{+}, HE_{11}^{-}, CV_{+1}^{+}, CV_{-1}^{-}, IV_{-1}^{+} and IV_{+1}^{-}), polarizer and observation screen. At first, let a fundamental mode $HE_{11}^{\sigma_1}$ and a single-charged OV ($CV_{\sigma_2}^{\sigma_2}$ or $IV_{-\sigma_2}^{\sigma_2}$, with $\sigma_{1,2} = \pm 1$) be present at the output end of the fibre. If the vortex is stable in case of the parabolic profile of the refractive index, the field could be written as

$$E_t = a(\hat{\mathbf{x}} + i\sigma_1\hat{\mathbf{y}})\exp\left\{-\frac{VR^2}{2} + i\beta_0 z\right\} + (\hat{\mathbf{x}} + i\sigma_2\hat{\mathbf{y}})R\exp\left\{-\frac{VR^2}{2} + i(\beta_1 z + \sigma_2\varphi)\right\}, \quad (8)$$

where a means the relative amplitude of the $HE_{11}^{\sigma_1}$ mode, $\hat{\mathbf{x}}$ and $\hat{\mathbf{y}}$ the unit linear polarization vectors, β the propagation constant of the mode and z the fibre length. When the polarizer is rotated by an angle $\theta = \Omega t$ (with t being the time and Ω the rotation frequency), the equation defining the position of zero-intensity point (ZIP) reads as follows:

$$a + R\exp\{i(\Delta\beta_{10} z + \sigma_2[\theta + \varphi] - \sigma_1\theta)\} = 0, \quad (9)$$

with $\Delta\beta_{10} = \beta_1 - \beta_0$. After equating real and imaginary parts in Eq. (9) to zero, one obtains the ZIP coordinates:

$$R = a, \varphi = (\pi - \Delta\beta_{10} z)\sigma_2 + (\sigma_1\sigma_2 - 1)\theta. \quad (10)$$

It is evident from Eq. (10) that the ZIP rotates even in the non-rotating coordinate system associated with the screen placed after rotating polarizer. The appropriate frequency is equal to

$$\Delta\omega = \frac{\partial\varphi}{\partial t} = (\sigma_1\sigma_2 - 1)\Omega. \quad (11)$$

Upon passing to coordinate system that co-rotates coupled with the polarizer, we have $\varphi' = \varphi - \theta$ and $\varphi = (\pi - \Delta\beta_{10} z)\sigma_2 + (\sigma_1\sigma_2 - 2)\theta$ for the angles, thus yielding in the following frequency of the ZIP motion:

$$\Delta\omega' = \frac{\partial\varphi'}{\partial t} = (\sigma_1\sigma_2 - 2)\Omega. \quad (12)$$

If $\sigma_1 = \sigma_2$, the singularity point does not rotate on a stationary screen. However, in case of $\sigma_1 = -\sigma_2$ one has $\Delta\omega = -2\Omega$ in the laboratory system, whereas the relation $\Delta\omega' = -3\Omega$ holds true for the rotating coordinate system.

If only the $HE_{11}^{\sigma_1}$ mode and the $IV_{-\sigma_2}^{\sigma_2}$ OV are present in the output field, the singularity point in the laboratory system would rotate with the frequency

$$\Delta\omega = \frac{\partial\varphi}{\partial t} = (1 - \sigma_1\sigma_2)\Omega, \quad (13)$$

and the relation

$$\Delta\omega' = \frac{\partial\varphi'}{\partial t} = -\sigma_1\sigma_2\Omega. \quad (14)$$

would be valid for the rotating coordinate system.

In the case of orthogonal polarizations of the $HE_{11}^{\sigma_1}$ mode and the $IV_{-\sigma_2}^{\sigma_2}$ vortex, the ZIP moves on a stationary screen with the angular frequency $\Delta\omega = 2\Omega$ and we have $\Delta\omega' = \Omega$ for the rotating screen. This difference in the angular frequencies for the CV and IV vortices is related to the difference in the total angular momenta of these fields.

In a real case, when the fibre is excited with right-handed circularly polarized light, the three circularly polarized modes HE_{11}^{+}, CV_{+1}^{+} and IV_{-1}^{+} are excited in it. Then one has to take into consideration that the OV IV_{-1}^{+} consists of two partial vortices [3],

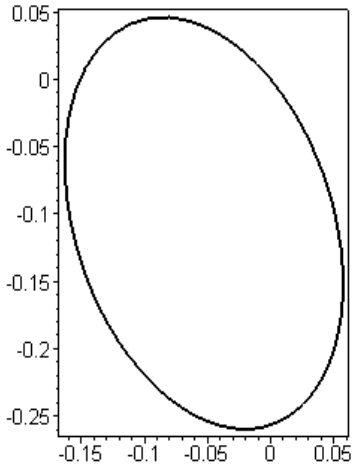

Fig. 4 Theoretical vortex trajectory produced by analyzer rotation. The coordinates are normalized with respect the core radius.

$$E_t\left(IV_{-1}^{+}\right)=\left\{\hat{\mathbf{e}}^{+}\exp(-i\varphi)\cos(\Delta\beta z)+i\hat{\mathbf{e}}^{-}\exp(i\varphi)\sin(\Delta\beta z)\right\}R\exp\left\{-\frac{VR^2}{2}+i\beta_2 z\right\}, \tag{15}$$

where $\Delta\beta z$ is the phase difference between the *TE* and *TM* modes the *IV* vortex consists of, and $\hat{\mathbf{e}}^{\pm}$ stand for the unit vectors of the circular polarizations. The field at the output face of fibre may be represented as

$$E_t=\left[a_0\hat{\mathbf{e}}^{+}+\hat{\mathbf{e}}^{+}R\exp\{i\varphi+\Delta\beta_{10}z\}+A_2R\left\{\hat{\mathbf{e}}^{+}\exp(-i\varphi)\cos(\Delta\beta z)+i\hat{\mathbf{e}}^{-}\exp(i\varphi)\sin(\Delta\beta z)\right\}\exp\{\Delta\beta_{20}z\}\right]$$
$$\times\exp\left\{-\frac{VR^2}{2}+i\beta_0 z\right\}. \tag{16}$$

The position of the singularity point after the polarizer is determined by the relations

$$\varphi=\arctan\frac{\sin\Phi_{10}+a_1\sin\Phi_{20}+a_2\sin(\Phi_{30}-2\theta)}{a_1\cos\Phi_{20}-a_2\cos(\Phi_{30}-2\theta)-\cos\Phi_{10}}, \tag{17}$$

$$R=\frac{a_0}{\cos\Phi_{10}-\sin\Phi_{10}\tan\varphi+a_1\cos\Phi_{20}-a_1\sin\Phi_{20}\tan\varphi+a_2\cos(\Phi_{30}-2\theta)-a_2\sin(\Phi_{30}-2\theta)\tan\varphi},$$

where $\Phi_{10}=\Delta\beta_{10}z$, $\Phi_{20}=\Delta\beta_{20}z$, $\Phi_{30}=\Delta\beta_{20}z+\pi/2$, $a_1=A_2\cos(\Delta\beta z)$ and $a_2=A_2\sin(\Delta\beta z)$. The obtained trajectory of the ZIP displayed in Fig. 4 has an elliptic form. The singularity point performs two cycles whenever the polarizer makes one revolution.

We have studied the vortex trajectory experimentally with the modified setup, in which the second quarter-wave plate is removed (see Fig. 2). We have photographed the intensity distributions after each polarizer rotation by the angle of 5°. The trajectory of the vortex is presented in Fig. 5.

4. Conclusions

Resulting from the results of investigations carried out above, one can make the following conclusions:

1. We have obtained both theoretically and experimentally the excitation coefficients for the guided OV occurring in ideal fibres. It is shown that, under the excitation by the OV, the beam displacement results in decreasing weight of the incident vortex and increasing weights of the fundamental mode and the oppositely charged vortex in the excited field.

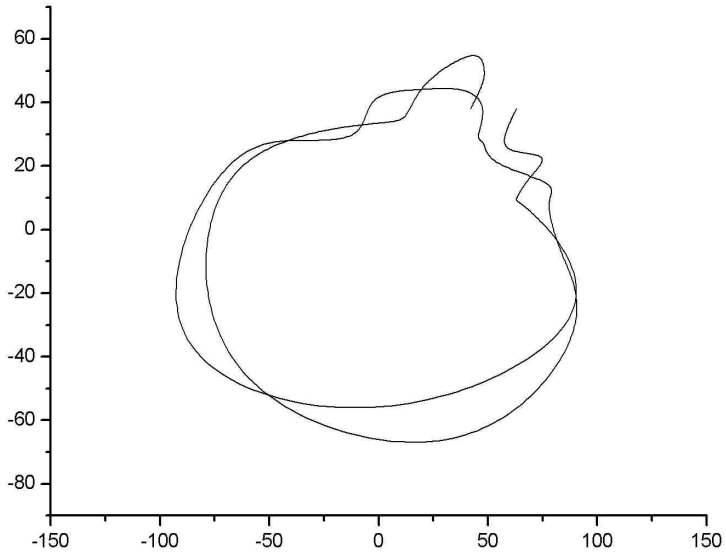

Fig. 5. Experimental vortex trajectory produced by analyzer rotation. The coordinates are measured in pixels.

2. In what the RDE manifestation in fibres concerns, the ZIP movement is affected not only by the topological charge of the vortex but also by the polarizations of the incident vortex and the fundamental mode, whose presence causes the displacement of the singularity point.
3. Excitation of fibres with circularly polarized light gives rise to elliptic form of the ZIP trajectory, along which the singularity point moves with the doubled frequency. The direction of that rotation is opposite to that of the polarizer in the case of right-handed circular polarization of the incident vortex with the positive topological charge.

References

1. Darsht M.Ya., Zel'dovich B.Ya., Katayevskaya I.V. and Kundikova N.D. Zhurn. Eksp. Teor. Fiz. **107** (1995) 464 (in Russian).
2. Bolshtyansky M.A. Opt. Spektrosk. **79** (1995) 512 (in Russian).
3. Volyar A.V. and Fadeyeva T.A. Opt. and Spectrosc. **85** (1998) 295.
4. Alekseev A.N., Volyar A.V. and Fadeeva T.A. Techn. Phys. Lett. **31** (2005) 374.
5. Fadeyeva T.A. and Volyar A.V. Techn. Phys. Lett. **29** (2003) 594.
6. Kerbage C., Westbrook P.S., Windeler R.S. and Eggleton B.J. Opt. & Photonics News **12** (2001) 18.
7. Mirovitsky D.I., Budagyan I.F. and Dubrovin V.F. Microwaveguiding optics and holography. "Nauka" Moskow (1983), 318 p. (in Russian).
8. Rybass A.F., Alexeyev A.N., Latysheva V.S. and Volyar A.V. Proc. CAOL **2** (2003) 57.
9. Allen L., Babiker M. and Power W.L. Opt. Commun. **112** (1994) 141.
10. Basistiy I. V., Bekshaev A.Ya., Vasnetsov M.V., Slyusar V.V. and Soskin M.S. JETP Lett. **76** (2002) 486.
11. Bekshaev A.Ya, Basistiy I.V., Slyusar V.V., Soskin M.S. and Vasnetsov M.V Ukr. J. Phys. **47** (2002) 1035 (in Ukrainian).
12. Snyder A. and Love J. Theory of optical waveguides, Chapman and Hall, London, New York, (1987).
13. Volyar A.V. and Fadeyeva T.A. Techn. Phys. Lett. **22** (1996) 69.
14. Izdebskaya Ya., Shvedov V., Kurabtzev D., Alexeyev A. and Volyar A. Proc. SPIE **4607** (2001) 78.